Progress in Neurobiology 205 (2021) 102120

Contents lists available at ScienceDirect

Progress in Neurobiology

journal homepage: www.elsevier.com/locate/pneurobio

Original Research Article

Functional organization of spatial frequency tuning in macaque V1 revealed with two-photon calcium imaging

Shu-Chen Guan [a,1], Nian-Sheng Ju [b,1], Louis Tao [b], Shi-Ming Tang [a,b,c,*], Cong Yu [a,c,d,*]

[a] PKU-Tsinghua Center for Life Sciences, Peking University, Beijing, China
[b] School of Life Sciences, Peking University, Beijing, China
[c] IDG-McGovern Institute for Brain Research, Peking University, Beijing, China
[d] School of Psychological and Cognitive Sciences, Peking University, Beijing, China

ARTICLE INFO

Keywords:
Primary visual cortex
Spatial frequency
Functional map
Two-photon imaging
Macaque

ABSTRACT

V1 neurons are functionally organized in orientation columns in primates. Whether spatial frequency (SF) columns also exist is less clear because mixed results have been reported. A definitive solution would be SF functional maps at single-neuron resolution. Here we used two-photon calcium imaging to construct first cellular SF maps in V1 superficial layers of five awake fixating macaques, and studied SF functional organization properties and neuronal tuning characteristics. The SF maps ($850 \times 850\ \mu m^2$) showed weak horizontal SF clustering (median clustering index = 1.43 vs. unity baseline), about one sixth as strong as orientation clustering in the same sets of neurons, which argues against a meaningful orthogonal relationship between orientation and SF functional maps. These maps also displayed nearly absent vertical SF clustering between two cortical depths (150 & 300 μm), indicating a lack of SF columnar structures within the superficial layers. The underlying causes might be that most neurons were tuned to a narrow two-octave range of medium frequencies, and many neurons with different SF preferences were often spatially mixed, which disallowed finer grouping of SF tuning. In addition, individual SF tuning functions were often asymmetric, having wider lower frequency branches, which may help encode low SF information for later decoding.

1. Introduction

V1 neurons are often functionally organized in orientation columns that group neurons with similar orientation preferences (Hubel and Wiesel, 1962, 1968), likely a result of wiring optimization (Chklovskii and Koulakov, 2004) or self-organization during evolvement (Kaschube et al., 2010). Although the roles of functional columns have been questioned (Horton and Adams, 2005), the local structures of orientation maps are found to be correlated to the tuning properties of neurons (Callaway, 1998; McLaughlin et al., 2003; Nauhaus et al., 2008; Li et al., 2019), which suggests that functional organizations may be related to different aspects of neural computation.

What has been less clear is the functional organization of V1 spatial frequency (SF) tuning. V1 neurons are also selective to stimulus SF (Campbell et al., 1969; Maffei and Fiorentini, 1977; De Valois et al., 1982). However, whether and how the SF tuning of V1 neurons are functionally organized remain debated (reviewed by Issa et al., 2008; Nauhaus et al., 2012). Results from single-unit recordings on SF tuning clustering are mixed. In cat area 17, DeAngelis et al. (1999) reported significant but weak SF clustering that was about 1/5 as strong as orientation clustering, and Tolhurst and Thompson (1982) and Molotchnikoff et al. (2007) found no clear SF clustering evidence. In Monkey V1, Silverman et al. (1989) discovered that neurons' different peak frequencies are distributed continuously and smoothly, consistent with their earlier 2-DG uptake results for SF columns (Tootell et al., 1988). Yet Edwards et al. (1995) described nearly even distributions of SF tuning from 1 to 6 cpd in blob to interblob cells, except some additional (~20 %) higher SF tuning in interblob cells, which would not support significant SF clustering. Intrinsic signal optical imaging (ISOI) studies, which target large-scale functional organizations of neural selectivities but lack single-neuron resolution, reveal either low and high SF preference regions (Hubener et al., 1997; Shoham et al., 1997; Kim et al., 1999), or more continuous clusters of SF tuning (Everson et al., 1998; Issa et al., 2000; Xu et al., 2007). However, it has been questioned

* Corresponding authors at: PKU-Tsinghua Center for Life Sciences, Peking University, Beijing, China.
E-mail addresses: tangshm@pku.edu.cn (S.-M. Tang), yucong@pku.edu.cn (C. Yu).
[1] Equal contribution co-first authors.

https://doi.org/10.1016/j.pneurobio.2021.102120
Received 21 February 2021; Received in revised form 6 June 2021; Accepted 8 July 2021
Available online 9 July 2021

that ISOI evidence for SF clusters could be spurious because of the influence of vascular artifacts (Sirovich and Uglesich, 2004).

Apparently a full understanding of the SF functional organization in V1 would benefit greatly from SF maps at single-neuron resolution, which is technically feasible with two-photon calcium imaging. A recent two-photon imaging study with calcium indicator dye Oregon Green BAPTA-1AM (OGB-1) revealed horizontal SF clustering and vertical SF columns in macaque V1 (Nauhaus et al., 2012), but the functional maps from large-scale imaging of this study were pixel-based with no cellular information (cellular details were only available with small-scale imaging in 200 × 200 μm^2 areas). To amend this issue, here we used long-term two-photon imaging with genetically encoded calcium indicators (GCaMP5) to construct first SF functional maps at single-neuron resolution in 5 awake macaque monkeys, using the methodology originally reported in Li et al. (2017). Our results revealed SF clustering in macaque V1 that was too weak to support a key conclusion of Nauhaus et al. (2012) that SF and orientation functional maps overlap orthogonally.

2. Materials and methods

The SF tuning data were collected from five rhesus monkeys (*Macaca mulatta*) aged at 5–8 years. The same monkeys' orientation tuning data, which were collected in the same sessions, have been reported in Ju et al. (2021). The details of materials and methods are repeated here for convenience. The only exception is the selection of SF tuned neurons, which replaced the selection of orientation tuned neurons in Ju et al. (2021).

2.1. Monkey preparation

Each monkey was prepared with two sequential surgeries under general anesthesia and strictly sterile conditions. In the first surgery, a 20-mm diameter craniotomy was performed on the skull over V1. The dura was opened and multiple tracks of 100−150 nl AAV1.hSynap. GCaMP5G.WPRE.SV40 (AV-1-PV2478, titer 2.37e13 (GC/mL), Penn Vector Core) were pressure-injected at a depth of ~350 μm. The dura was then sutured, the skull cap was re-attached with three titanium lugs and six screws, and the scalp was sewn up. After the surgery, the animal was returned to the cage, treated with injectable antibiotics (Ceftriaxone sodium, Youcare Pharmaceutical Group, China) for one week. Postop analgesia was also administered. The second surgery was performed 45 days later. A T-shaped steel frame was installed for head stabilization, and an optical window was inserted onto the cortical surface. More details of the preparation and surgical procedures can be found in Li et al. (2017). The procedures were approved by the Institutional Animal Care and Use Committee, Peking University.

2.2. Behavioral task

After a ten-day recovery from the second surgery, monkeys were seated in primate chairs with head restraint. They were trained to hold fixation on a small white spot (0.1°). The eye positions were monitored by an ISCAN ETL-200 infrared eye-tracking system (ISCAN Inc.) at a 120-Hz sampling rate. During the experiment, trials with eye positions deviated 1.5° or more from the fixation were discarded as ones with saccades and were repeated. The mean and standard deviation of the eye positions from the fixation point were 0.18° and 0.16° for monkey A, 0.37° and 0.32° for monkey B, 0.22° and 0.12° for monkey C, 0.16° and 0.28° for monkey D, and 0.23° and 0.20° for monkey E. The eye positions were within 0.5° from the fixation point in 96.5 % of trials for Monkey A, 74.4 % for Monkey B, 97.4 % for Monkey C, 95.5 % for Monkey D, and 92.9 % for Monkey E.

2.3. Visual stimuli

Visual stimuli were generated by the ViSaGe system (Cambridge Research Systems) and presented on a 21'' CRT monitor (SONY G520). The monitor resolution was 1280 pixel × 960 pixel, and the refresh rate was 80 Hz. Limited by the space and the monitor size, the viewing distance was varied with the stimulus spatial frequency (30 cm at 0.25/0.5/1cpd, 60 cm at 2cpd, and 120 cm at 4/8 cpd).

A drifting square-wave grating (3 cycles/s, full contrast, 4 cpd spatial frequency, and 0.4° diameter in size) was first used to determine the population receptive field location and size associated with a recording FOV (field of view) at 2−4° eccentricity, as well as ocular dominance columns when monocularly presented to confirm the V1 location. This process was quick with the use of a 4 × objective lens mounted on the two-photon microscope, which revealed no cell-specific information.

Cell-specific responses were then measured with a high-contrast (0.9) Gabor grating (Gaussian-windowed sinusoidal grating) drifting at 2 cycles/s in opposite directions perpendicular to the Gabor orientation. The Gabor grating varied at 12 equal-spaced orientations from 0° to 165° in 15° steps, and 6 spatial frequencies from 0.25 to 8 cpd in 1-octave steps. In addition, our pilot measurements suggested very strong surround suppression with larger stimuli. Therefore, we used three stimulus sizes at each spatial frequency, so as to estimate the best responses of each neuron with the most RF center summation and least surround suppression. Specifically, the σ of the Gaussian envelop of the Gabor were 0.64λ and 0.85λ at all SFs, and was additionally smaller at 0.42λ when SFs were 0.25, 0.5, and 1 cpd, and larger at 1.06λ when SFs were 2, 4, and 8 cpd (λ: wavelength; Gabors with the same σ in wavelength unit had the same number of cycles). Here at the smallest σ (0.42λ), the Gabors still had sufficient number of cycles (frequency bandwidths = 1 octave) (Graham, 1989), so that the actual stimulus SFs were precise at nominal values.

Each stimulus was presented for 1 s, with an inter-stimulus interval (ISI) of 1000 ms (Monkeys A & B) or 1500 ms (Monkeys C-E). After an ISI of 1000 ms, neural responses to optimal stimulus conditions were not fully back to the baseline level, which would affect F0 of the next trial, but this issue was minimized when the ISI was extended to 1500 ms (Ju et al., 2021). Each stimulus condition was repeated 10 times for Monkeys A & B, and 12 times for Monkeys C-E, with half trials for each opposite direction. Imaging of neuronal responses at a specific FOV and depth (e.g., Monkey A1_150 μm) including all orientations, SFs, and sizes was completed in one session that lasted 3 – 4 hours. During the session, recording at a specific viewing distance was completed before moving to the next distance, with all stimulus conditions at that distance pseudo-randomly presented.

2.4. Two-photon imaging

Two-photon imaging was performed with a Prairie Ultima IV (In Vivo) two-photon microscope (Prairie Technologies) and a Ti:sapphire laser (Mai Tai eHP, Spectra Physics). During imaging, a 16 × objective lens (0.8 N.A., Nikon) with a resolution of 1.6 μm/pixel was used, along with 1000-nm femtosecond laser. A fast resonant scanning mode (32 fps) was chosen to obtain continuous images of neuronal activities (8 fps after averaging every 4 frames). One or two FOVs of 850 × 850 μm^2 were selected in each animal. Recordings at two depths for the same FOV were completed in two consecutive days. On the first day, imaging were performed at 150 μm, and some neurons with high brightness or unique dendrite patterns were selected as landmarks. On the second day, the same FOV at 150 μm was located with the help of landmark neurons. Then the depth plane was lowered to 300 μm to start new recording. This procedure was not strictly followed when imaging was performed at A2, which produced two misaligned FOVs (see Fig. 2A).

2.5. Data analysis: initial screening of ROIs

Data were analyzed with customized MATLAB codes. A normalized cross-correlation based translation algorithm was used to correct motion artifacts (Li et al., 2017). After the correction, fluorescence changes were associated with corresponding visual stimuli through the time sequence information recorded by Neural Signal Processor (Cerebus system, Blackrock Microsystem). By subtracting the mean of the 4 frames before stimuli onset (*F0*) from the average of the 6th-9th frames after stimuli onset (*F*) across 5 or 6 repeated trials for the same stimulus condition (same orientation, spatial frequency, size, and drifting direction), the differential image ($\Delta F = F - F0$) was obtained.

The regions of interest (ROIs) or possible cell bodies were decided through sequential analysis of 216 differential images in the order of SF (6), size (3), and orientation (12) ($6 \times 3 \times 12 = 216$). The first differential image was filtered with a band-pass Gaussian filter (size = 2–10 pixels), and connected subsets of pixels (>25 pixels, which would exclude smaller vertical neuropils) with the mean pixel value > 3 standard deviations of the mean brightness were selected as ROIs. Then the areas of these ROIs were set to mean brightness in the next differential image before the bandpass filtering and thresholding were repeated (This measure would eventually reduce the SDs of differential images and facilitate detection of neurons with relatively low fluorescence responses). If a new ROI and an existing ROI from the previous differential image overlapped, the new ROI would be on its own if the overlapping area OA < 1/4 ROI_{new}, discarded if 1/4 ROI_{new} < OA < 3/4 ROI_{new}, and merged with the existing ROI if OA > 3/4 ROI_{new}. The merges would help smooth the contours of the final ROIs. This process went on through all 216 differential images twice to select ROIs. Finally, the roundness for each ROI was calculated as:

$$Roundness = \frac{\sqrt{4\pi \times A}}{P}$$

where *A* was a ROI's area, and *P* was the perimeter. Only ROIs with roundness larger than 0.9, which would exclude horizontal neuropils, were selected as neurons for further analysis.

2.6. Data analysis: selection of SF-tuned neurons

The ratio of fluorescence change ($\Delta F/F0$) was calculated as a neuron's response to a specific stimulus condition. For a specific neuron's response to a specific stimulus condition, the $F0_n$ of the n-th trial was the average of 4 frames before stimulus onset, and F_n was the average of 5th-8th or 6th-9th frames after stimulus onset, whichever was greater (Later analysis found that if the time window was fixed at 5th-8th frames, on average the number of neurons per map increased from 729 to 750, and the median horizontal clustering index CI changed from 1.43 to 1.47, which had little impacts on the overall results and conclusions). $F0_n$ was then averaged across 10 or 12 trials to obtain the baseline F0 for all trials (for the purpose of reducing noises in the calculation of responses), and $\Delta F_n/F0 = (F_n\text{-}F0)/F0$ was taken as the neuron's response to this stimulus at this trial. Only a small portion (~3%) of superficial-layer neurons showed direction selectivity as their responses to two opposite directions differed significantly ($p < 0.05$, non-parametric Friedman test), which was consistent with previous estimates with single-unit recording and two-photon imaging in macaques (Livingstone and Hubel, 1984; Gur and Snodderly, 2008; Ikezoe et al., 2013). For those neurons, the 5-6 trials at the preferred direction was considered for calculation of $\Delta F_n/F0$ as the neuron's responses to a particular stimulus. F0 was still averaged over 10–12 trials at two opposite directions.

Several steps were then taken to decide whether each neuron was tuned to spatial frequency. (1) The optimal orientation, SF, and stimulus size producing the maximal response among all conditions were selected. Then responses to other five SFs were decided at the same orientation and stimulus size. (2) To select SF tuned neurons, a non-parametric Friedman test was first performed to test whether a neuron's responses at 6 SFs were significantly different from each other ($\alpha = 0.05$). (3) For those showing significant difference, the SF tuning function of each neuron was fitted with a Different-of-Gaussian model.

$$R(sf) = a_1 e^{-\left(\frac{sf}{\sigma_1}\right)^2} - a_2 e^{-\left(\frac{sf}{\sigma_2}\right)^2} + b$$

where R(sf) was a neuron's response at spatial frequency sf, free parameters a_1, σ_1, a_2, and σ_2 were amplitudes and standard deviations of two Gaussians, respectively, and b was the minimal response among six SFs. Only neurons with goodness of fit $R^2 > 0.5$ were used in data analysis because both preferred SF and tuning bandwidth could be revealed with data fitting. A separate analysis found that the SF clustering indices within the same maps (Fig. 2B) were reduced by less than 4% when all SF selective neurons were considered regardless of R^2.

3. Results

We recorded neuronal responses to a Gabor grating of various SFs (0.25–8 cpd) and orientations in V1 superficial layers of five awake, fixating macaques. Neurons were sampled at two depths (150 and 300 μm deep from the cortical surface) and at 2−4° eccentricity. Imaging processing and data analysis identified a total of 10205 neurons that were tuned to SF (see Fig. 1 for example neurons and data fitting). The functional maps and tuning properties of these neurons are described below. The orientation results have been published in a separate paper (Ju et al., 2021).

3.1. SF functional maps

Unlike orientation functional maps built from the same data sets that showed significant orientation clusters and columns (Ju et al., 2021), SF functional maps suggested weak horizontal SF clustering and nearly absent vertical SF clustering within V1 superficial layers (Fig. 2A).

To characterize horizontal SF clustering at the same cortical depth quantitatively, for each SF map we calculated the difference of preferred frequencies (DPSFs) of each neuron pair as a function of their absolute cortical distance, as well as the baseline with neuron positions shuffled (Fig. 2B left). The degree of SF clustering was then indicated by a clustering index (CI), which was the inverse of $DPSF_{mean}/DPSF_{baseline}$ (Fig. 2B middle). For all SF maps, the range of CIs within the first 50 μm of cortical distance was [1.17 2.17], with a median of 1.43. In comparison, the corresponding CI range of orientation tuning was [2.53 5.19], with a median of 3.57 (Ju et al., 2021). Therefore, median SF clustering was $(CI_{SF} - 1)/(CI_{ORI} - 1) = 16.1$ %, or approximately 1/6 of orientation clustering. This sharp difference can be appreciated in Fig. 2B (right panel) where SF and orientation CIs of individual recording FOVs (averaged over two cortical depths) are contrasted. Indeed, if the threshold for clustering is arbitrarily set at CI = 2.0, which is about two thirds (i.e., $(2.0 - 1)/(2.53 - 1) = 0.65$) of the lowest orientation CI at 2.53, then only A1_300 (i.e., Map A1 at 300 μm; CI = 2.06) and D_300 (CI = 2.13) are above the threshold.

Moreover, the between-depth pairwise DPSFs were nearly identical to baselines in most recording FOVs (Fig. 2C left; A2 excluded due to misaligned maps). Here each pair included one neuron from 150 μm and the other from 300 μm depth. The CI range within the first 50 μm of cortical distance was [0.94 1.63], with a median of 1.00, suggesting likely absence of vertical SF clustering within the superficial layers (Fig. 2C middle). In contrast, corresponding CIs for orientation clustering across the same two depths were robust (median = 3.17, replotted in Fig. 2C right from Ju et al. (2021)). In addition, there was no horizontal clustering of SF tuning bandwidth (Fig. 2D), as the range of CIs within the first 50 μm of cortical distance was [0.94 1.30], and the median CI was 1.02.

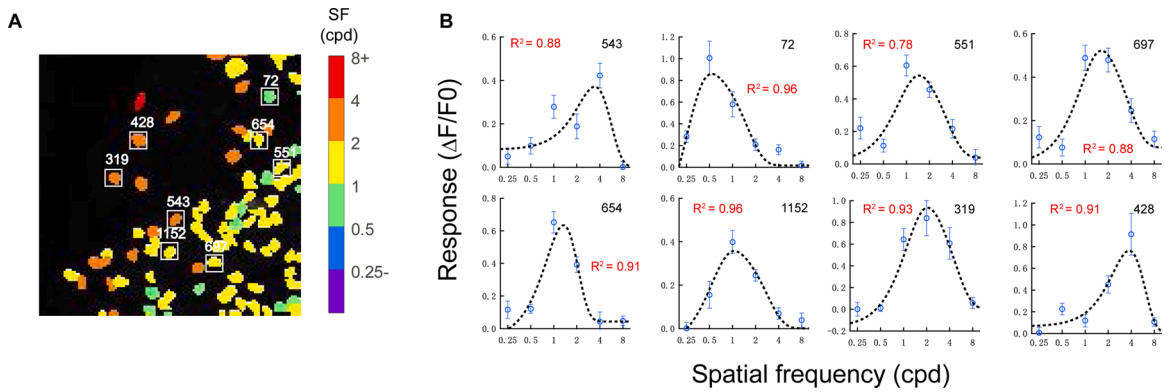

Fig. 1. Examples of SF tuned neurons from Monkey A. **A**. Zoomed-in view of the outlined area in the SF map of Monkey A FOV 1 at 150 μm cortical depth (A1_150) in Fig. 2A. The colors indicate the preferred SFs of neurons. Eight example neurons are marked with squares and neuron IDs. **B**. The SF tuning functions of eight example neurons and their Difference-of-Gaussian fittings. R^2 indicates the goodness-of-fit. Error bars represent ±1 SEM.

3.2. SF preferences

Neurons in each SF map appeared to mostly prefer a limited range of SFs (Fig. 2A). In Maps A1, A2, C1, and C2 at both depths, neurons were mainly tuned to medium SFs, and those in Maps B, D, and E at both depths were mainly tuned to higher SFs. The percentage distribution plots suggest that most neurons in each SF map were tuned to a 2-octave SF range (Fig. 3A), consistent with electrophysiological estimates (De Valois et al., 1982). Take A1 for example, 84.0 % neurons' preferred SFs fell into a 2-octave range (0.99–3.97 cpd) at 150 μm, and 94.1 % at 300 μm (1.04–4.17 cpd). On average 86.1 % of neurons from all maps were tuned to a 2-octave range of SFs. These limited ranges of SF preference, plus frequently mingled positions of neurons tuned to different SFs (Fig. 2A), often made it difficult for neurons' SF preferences to be further divided into distinct and finer SF clusters.

The SF preferences appeared to be stable beyond the limited areas of FOVs in the same animals. Fig. 3B compared preferred SFs in FOVs A1 and A2 in Monkey A that were slightly overlapping at one corner, and C1 and C2 in Monkey C that were separated by approximately 300 μm (Fig. S1). In both animals, the median preferred SFs differed by 1 octave or less between two adjacent FOVs at 150 μm, and were virtually unchanged at 300 μm (around 2 cpd). These limited results suggested that, besides the limited ranges of SF tuning within FOVs, neurons likely also preferred similar ranges of SFs over longer distances.

Higher visual areas are known to prefer lower SFs as stimulus processing becomes more global (De Valois et al., 1982; Foster et al., 1985; Desimone and Schein, 1987). We examined whether this trend also holds within the superficial layers of V1. Some FOVs did show clear shifts of SF preferences from higher to lower SFs at more superficial cortical depths (Fig. 3B; A2 excluded due to misalignment). More neurons were tuned to lower median SFs at 150 μm than at 300 μm in A1, B, C2, and D (Fig. 3C), even if these neurons were in the same orientation columns with similar orientation preferences (vertical orientation CI = 3.51, 3.93, 2.52, and 3.17, respectively; Fig. 2C bottom). However, the preferred SFs at two cortical depths were similar in C1 and E. More data are thus needed to reveal whether there are true high-to-low shifts of preferred SFs within the superficial layers.

3.3. SF tuning bandwidth

The median SF tuning bandwidth at half height (i.e., $\log_2(SF_{high}/SF_{low})$) ranged 1.93–3.22 octaves among maps, with the grand median of all neurons being 2.01 octaves at 150 μm and 1.99 octaves at 300 μm ($p = 0.608$, Wilcoxon rank sum test; Fig. 3D). Neurons in SF maps B and E at both depths had wider bandwidths (2.24–3.18 octaves), which might have been overestimated because over 20 % of B and E neurons were categorized as high-pass (Fig. 3A) and assigned infinite bandwidth. However, some of these high-pass neurons might actually be band-pass if their responses to higher SFs had been tested. Overall the estimated SF tuning bandwidths were wider than the single-unit data of 1.32 octaves for simple cells and 1.60 octaves for complex cells in parafovea (De Valois et al., 1982), but were consistent with one psychophysical estimate (Wilson et al., 1983).

Psychophysical and single-unit recording evidence has indicated that the SF tuning bandwidth decreases with preferred SF of spatial channels or V1 neurons (De Valois et al., 1982; Wilson et al., 1983). This was also demonstrated here in that the SF tuning bandwidth reduced as a function of the preferred SF (Fig. 3E). Log-linear regressions ($y = a + b*\log(x)$; y for SF tuning bandwidth, x for preferred SF, and b for slope) revealed negative slopes. The median slope was -0.29 among all SF maps, significantly different from 0 ($p < 0.001$, Wilcoxon signed-rank test).

3.4. Asymmetric SF tuning functions

Noticing that many SF tuning functions were asymmetric (Fig. 1B), often containing wider low-frequency branches, we calculated high half bandwidth at half height ($HhBW = \log_2(SF_{high}/SF_{peak})$) and low half bandwidth at half height ($LhBW = \log_2(SF_{peak}/SF_{low})$) for each tuning function (Fig. 4A). Take A1_150 as an example, the median HhBW and LhBW were 0.78 and 1.17 octaves, respectively, differing by 0.39 octaves (Fig. 4B). This trend was evident in eleven maps (Fig. 4B) but not the remaining three (B_300, E_150, and E_300) where HhBWs were either wider than or similar to LhBWs. However, these latter estimates of B_300, E_150, and E_300 might be inaccurate. As we argued earlier, some high-pass neurons might be actually bandpass neurons if higher SFs had been tested. The asymmetric SF functions may help downstream visual areas encode low SF information, which will be discussed later.

4. Discussion

In this study we used two-photon calcium imaging to investigate SF functional organization and associated neuronal tuning properties in V1 superficial-layers of awake, fixating macaques. At single neuron resolution, SF maps showed weak horizontal SF clustering that was about 1/6 as strong as orientation clustering from the same sets of neurons. Most neurons in each SF map were tuned to a narrow two-octave range of medium frequencies. Moreover, neurons with different SF preferences were often spatially mingled. The narrow tuning range and the spatial mingling together reduced the possibility of neurons forming distinct and finer SF clusters. Vertical SF clustering was nearly absent within V1 superficial layers, although the same neurons displayed significant vertical orientation clustering. Whether SF tuning lacks columnar structures entirely requires data at greater cortical

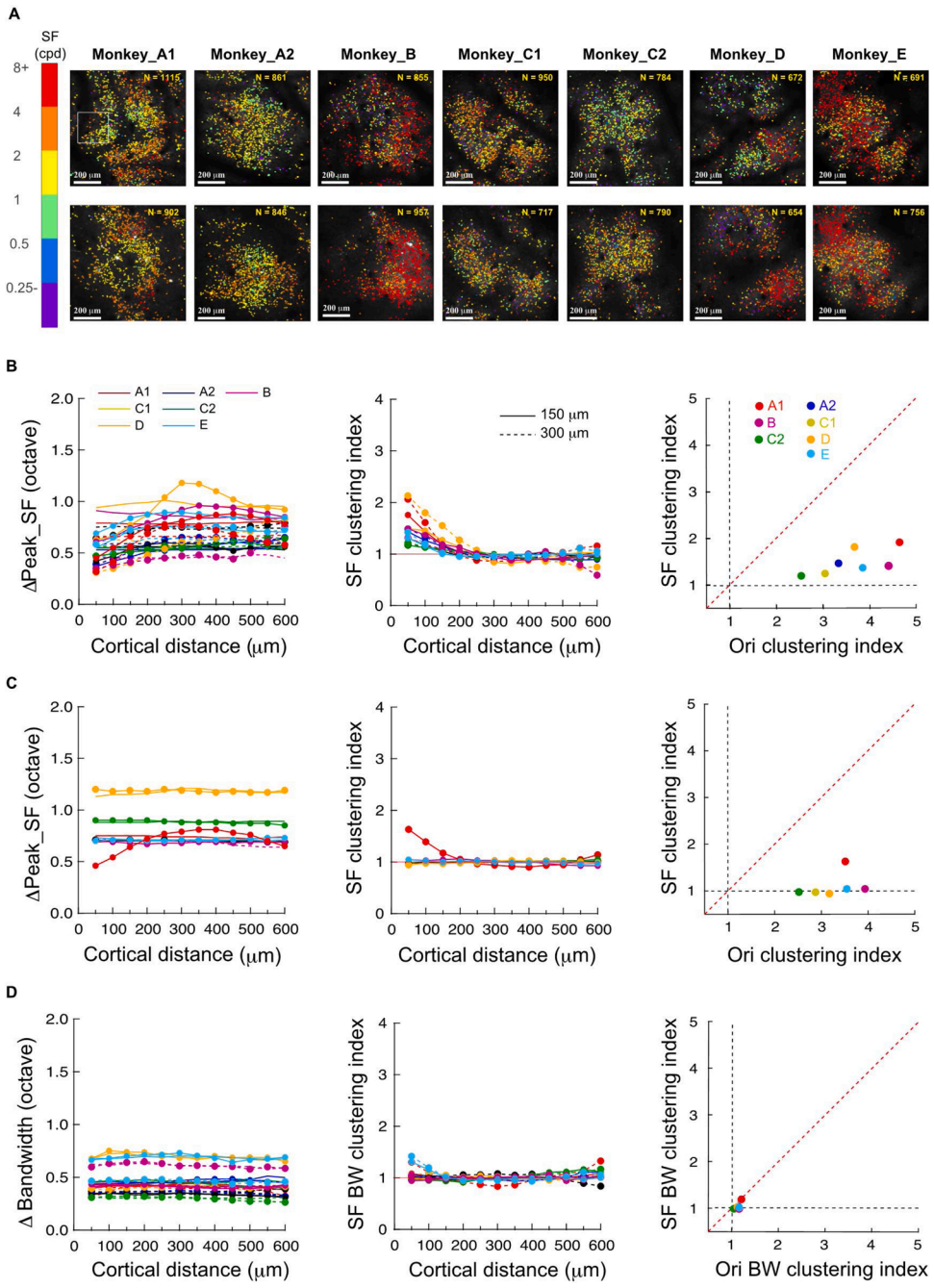

Fig. 2. SF functional maps. **A**. SF maps at 150 and 300 μm cortical depths. A Zoomed-in view of the outlined area in A1_150 μm is shown in Fig. 1A. **B**. Horizontal SF clustering within the same map. Left: Mean pairwise difference of preferred SFs (DPSF) as a function of the absolute cortical distance. Each datum indicates the average pairwise DPSF within a 50-μm bin up to the corresponding cortical distance on the x-axis. Each corresponding baseline (same color and line style but no symbols) represents simulated pairwise DPSFs with neurons shuffled in position. Middle: The SF clustering index within each 50-μm bin of cortical distance. The index was defined as the inverse of $DPSF_{mean}/DPSF_{baseline}$. Right: SF vs. orientation clustering indices within the first 50-μm bin of cortical distance (CIs averaged over two depths). **C.** Vertical SF clustering across depths. Left: Mean across-depth pairwise DPSF as a function of the absolute cortical distance. Plots are the same as in **B** except that the two neurons in each pair are drawn from maps at 150 and 300 μm depths, respectively. A2 was excluded due to misaligned maps. Middle: The SF tuning clustering index within each 50-μm bin of cortical distance. Right: SF vs. orientation clustering indices within the first 50-μm bin of cortical distance. **D**. SF tuning bandwidth clustering within the same depth. Left: Mean pairwise difference of SF tuning bandwidth (DBW) as a function of the absolute cortical distance. Each datum indicates the average pairwise difference within a 50-μm bin up to the corresponding cortical distance on the x-axis. Each corresponding baseline (same color and line style but no symbols) represents simulated pairwise DBWs with neurons shuffled in position. Middle: The SF tuning bandwidth clustering index within each 50-μm bin of cortical distance. Right: SF vs. orientation tuning bandwidth clustering indices within the first 50-μm bin of cortical distance. The orientation data were replotted from Ju et al. (2021). Error bars represent ±1 SEM.

depths, which is difficult with current two-photon imaging technology.

Our results are largely consistent with several electrophysiological reports that SF clustering is weak or insignificant in cat area 17 and macaque V1 (Tolhurst and Thompson, 1982; Edwards et al., 1995; DeAngelis et al., 1999; Molotchnikoff et al., 2007). However, they are in contrary to the report of distinct 2-DG uptakes with low and high SF stimuli in respective V1 blob and interblob regions by Tootell et al. (1988), and to their subsequent single-unit findings of continuous and smooth transitions of preferred SFs over a cortical distance of 0.6–0.7 mm (Silverman et al., 1989). It is unclear why our two-photon results are consistent with some early reports but not the ones from the De Valois group. Nevertheless, our two-photon imaging study and De Valois et al. (1982) both revealed that most parafoveal neurons in macaque V1 prefer a 2-octave range of medium SFs. As discussed above, the limited range of SF tuning may have contributed to weak SF clustering.

Our results also differed from those in an earlier two-photon imaging study (Nauhaus et al., 2012). The latter reported distinct SF clusters in similarly-sized (800 × 800 μm^2) but pixel-based SF maps in macaque V1 superficial layers. Moreover, in their 200 × 200 μm^2 "micro-maps" with single-neuron resolution, the SF clustering index was about 60 % of the orientation clustering index in an exemplar map and about 40 % when all 735 neurons in 10 imaging regions were pooled. The stimuli used in two studies were not very different (2–8 Hz drifting gratings at SFs of 0.5–8 cpd vs. our 2-Hz drifting gratings at SFs of 0.25–8 cpd). It is unclear what exactly caused the discrepancies, although we suspect that several factors might have contributed. First, in Nauhaus et al. (2012), the image resolution was ~3 μm per pixel, lower than 1.6 μm per pixel of ours. Each pixel in their pixel-based SF maps averaged not only calcium responses of cell bodies and neuropils, but also likely different SF preferences of nearby neurons due to lower resolution, leading to inflated

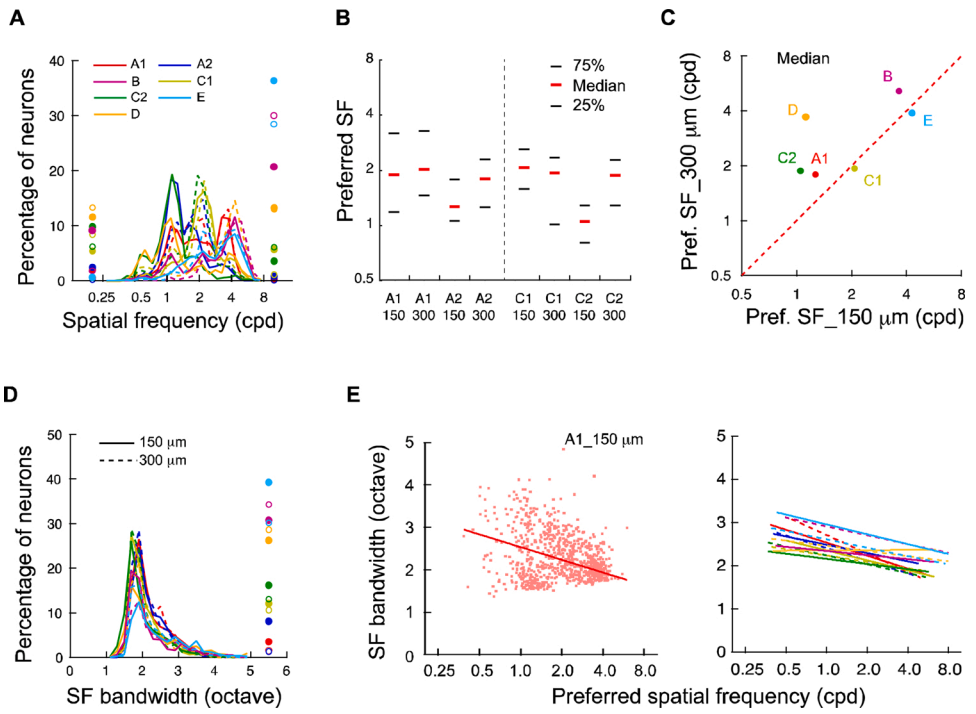

Fig. 3. SF tuning properties in V1 superficial-layer neurons. **A**. The percentage distribution of neurons against preferred SF in each map. Isolated filled and open circles indicate the percentages of low-pass (left side) and high-pass (right side) neurons on the basis of data fitting at 150 and 300 μm cortical depths, respectively. **B**. SF preference distributions of adjacent SF maps A1 and A2, and of C1 and C2, at 150 and 300 μm cortical depths, respectively. **C**. The median preferred SFs at 150 μm vs. 300 μm in each SF map (A2 excluded due to misalignment). **D**. The percentage distribution of neurons against SF tuning bandwidth in each map. Isolated filled and open circles on the right side indicate the summed percentages of low-pass and high-pass neurons at 150 and 300 μm cortical depths, respectively. **E**. SF tuning bandwidth vs. preferred SF. The left panel shows individual neurons' data and the loglinear regression of Map A1_150. The right panel shows loglinear regression lines of all maps.

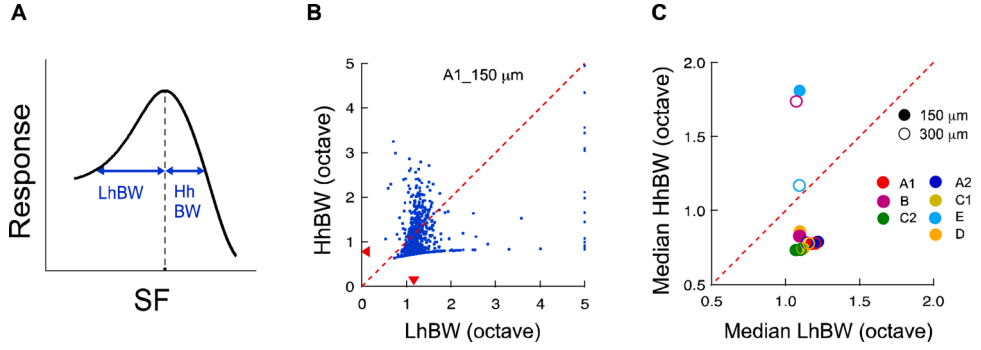

Fig. 4. Asymmetric SF tuning functions. **A**. Illustrations of lower- and higher-half bandwidths at half height (LhBW & HhBW). **B**. LhBW vs. HhBW of each neuron in Map A1_150. Red arrows indicate medians. **C**. Median LhBW vs. HhBW of each map.

appearance of SF clustering. Our Fig. S2 demonstrates this trend of inflated SF clustering in some pixel-based SF maps constructed with the same method and imaging resolution of Nauhaus et al. (2012). Second, Nauhaus et al. (2012) presented different stimulus conditions with zero time gaps, likely because of the time constraints posed by the use of toxic calcium indicator dye. As a result, the slow calcium signals from preceding trials inevitably interfered with those of later trials, which would smear the SF preferences of neighboring neurons and enhance SF clustering to certain degree. Third, the SF clustering indices in Nauhaus et al. (2012) might be biased by relatively small numbers of neurons pooled from multiple images. In contrast, our estimates are likely less biased on the basis of 14 SF maps and a total of 10k neurons.

The exact SF range varied among maps (Fig. 2A). These variations were unrelated to retinal eccentricity, as FOVs in Monkeys B, D and E, which showed higher preferred SFs, were not closer to the fovea than those in Monkeys A and C. Other possibilities included individual differences of SF preferences among monkeys, sampling biases in the same monkey, and SF clustering in a grander scale than orientation tuning. Fig. 3B showed similar SF tuning across adjacent FOVs A1 and A2, and across C1 and C2, in two macaques, which was inconsistent with sampling bias and grander SF clustering. Emergent large-FOV two-photon imaging technology (e.g., Ota et al., 2021) would provide more definitive solutions to these issues.

Hubel and Wiesel first suggested that orientation, eye of origin, and retinal location can be uniformly represented with optimal (orthogonal) overlay of orientation and ocular dominance maps (Hubel and Wiesel, 1977). This uniform representation becomes more challenging when additional functional maps such as direction and disparity maps are considered (Swindale, 2000; Horton and Adams, 2005). One implication of our findings is that orientation and SF maps can hardly maintain a meaningful orthogonal relationship (Nauhaus et al., 2012) since there is not much SF clustering to begin with. As a result, including SF to the uniform representation of stimulus features does not add further burden to the already complex superpositions of functional maps.

Neurons in our SF maps were seldomly tuned to low SFs or low pass, even if macaques, like humans, are sensitive to low SF stimuli (De Valois et al., 1974). Differential neural responses to bright and dark regions of low-SF stimuli may represent the low-SF information (Benvenuti et al., 2018). Alternatively, the wider low-half bandwidth (LhBW) of SF tuning functions in most neurons (Fig. 4) suggests that low SF information may be picked up by medium-frequency neurons. This possibility is supported by psychophysical adaptation and masking results that a lowpass

SF filter handles all SF information at the filter's preferred and lower SFs (Blakemore and Campbell, 1969; Wilson et al., 1983). The low SF information may then be decoded by later V2 neurons whose preferred SFs are 2-octave lower than those of V1 neurons (Foster et al., 1985). Imagine that a low-SF stimulus is responded by two V1 neurons tuned to the same medium SF, and their SF tuning functions are identical in HhBW but differ in LhBW, a subtraction of two tuning functions by a V2 neuron would produce a low-SF peak.

Acknowledgments

This study was supported by Natural Science Foundation of China grants 31230030 and 31730109, and funds from Peking-Tsinghua Center for Life Sciences, Peking University. We thank Geoff Ghose, Stanley Klein, Haidong Lu, Guy Orban, Adam Reeves, and Rufin Vogels for their very helpful comments and suggestions.

Appendix A. The Peer Review Overview and Supplementary data

The Peer Review Overview and Supplementary data associated with this article can be found in the online version, at doi:https://doi.org/10.1016/j.pneurobio.2021.102120.

References

Benvenuti, G., Chen, Y., Ramakrishnan, C., Deisseroth, K., Geisler, W.S., Seidemann, E., 2018. Scale-invariant visual capabilities explained by topographic representations of luminance and texture in primate V1. Neuron 100 (1504-1512), e1504.
Blakemore, C., Campbell, F.W., 1969. On the existence of neurones in the human visual system selectively sensitive to the orientation and size of retinal images. J. Physiol. 203, 237–260.
Callaway, E.M., 1998. Local circuits in primary visual cortex of the macaque monkey. Annu. Rev. Neurosci. 21, 47–74.
Campbell, F.W., Cooper, G.F., Enroth-Cugell, C., 1969. The spatial selectivity of the visual cells of the cat. J. Physiol. 203, 223–235.
Chklovskii, D.B., Koulakov, A.A., 2004. Maps in the brain: what can we learn from them? Annu. Rev. Neurosci. 27, 369–392.
De Valois, R.L., Morgan, H., Snodderly, D.M., 1974. Psychophysical studies of monkey vision. 3. Spatial luminance contrast sensitivity tests of macaque and human observers. Vision Res. 14, 75–81.
De Valois, R.L., Albrecht, D.G., Thorell, L.G., 1982. Spatial frequency selectivity of cells in macaque visual cortex. Vision Res. 22, 545–559.
DeAngelis, G.C., Ghose, G.M., Ohzawa, I., Freeman, R.D., 1999. Functional micro-organization of primary visual cortex: receptive field analysis of nearby neurons. J. Neurosci. 19, 4046–4064.
Desimone, R., Schein, S.J., 1987. Visual properties of neurons in area V4 of the macaque: sensitivity to stimulus form. J. Neurophysiol. 57, 835–868.
Edwards, D.P., Purpura, K.P., Kaplan, E., 1995. Contrast sensitivity and spatial frequency response of primate cortical neurons in and around the cytochrome oxidase blobs. Vision Res. 35, 1501–1523.
Everson, R.M., Prashanth, A.K., Gabbay, M., Knight, B.W., Sirovich, L., Kaplan, E., 1998. Representation of spatial frequency and orientation in the visual cortex. Proc. Natl. Acad. Sci. U. S. A. 95, 8334–8338.
Foster, K.H., Gaska, J.P., Nagler, M., Pollen, D.A., 1985. Spatial and temporal frequency selectivity of neurones in visual cortical areas V1 and V2 of the macaque monkey. J. Physiol. 365, 331–363.
Graham, N., 1989. Visual Pattern Analyzers (Oxford Psychology Series, No. 16). Oxford University Press, New York.
Gur, M., Snodderly, D.M., 2008. Physiological differences between neurons in layer 2 and layer 3 of primary visual cortex (V1) of alert macaque monkeys. J. Physiol. 586, 2293–2306.
Horton, J.C., Adams, D.L., 2005. The cortical column: a structure without a function. Philos. Trans. R. Soc. Lond. B Biol. Sci. 360, 837–862.
Hubel, D.H., Wiesel, T.N., 1962. Receptive fields, binocular interaction and functional architecture in the cat's visual cortex. J. Physiol. 160, 106–154.
Hubel, D.H., Wiesel, T.N., 1968. Receptive fields and functional architecture of monkey striate cortex. J. Physiol. 195, 215–243.
Hubel, D.H., Wiesel, T.N., 1977. Ferrier lecture. Functional architecture of macaque monkey visual cortex. Proc. R. Soc. Lond. B Biol. Sci. 198, 1–59.
Hubener, M., Shoham, D., Grinvald, A., Bonhoeffer, T., 1997. Spatial relationships among three columnar systems in cat area 17. J. Neurosci. 17, 9270–9284.
Ikezoe, K., Mori, Y., Kitamura, K., Tamura, H., Fujita, I., 2013. Relationship between the local structure of orientation map and the strength of orientation tuning of neurons in monkey V1: a 2-photon calcium imaging study. J. Neurosci. 33, 16818–16827.
Issa, N.P., Trepel, C., Stryker, M.P., 2000. Spatial frequency maps in cat visual cortex. J. Neurosci. 20, 8504–8514.
Issa, N.P., Rosenberg, A., Husson, T.R., 2008. Models and measurements of functional maps in V1. J. Neurophysiol. 99, 2745–2754.
Ju, N., Guan, S.C., Tao, L., Tang, S.M., Yu, C., 2021. Orientation tuning and end-stopping in macaque V1 studied with two-photon calcium imaging. Cereb. Cortex 31, 2085–2097.
Kaschube, M., Schnabel, M., Lowel, S., Coppola, D.M., White, L.E., Wolf, F., 2010. Universality in the evolution of orientation columns in the visual cortex. Science 330, 1113–1116.
Kim, D.S., Matsuda, Y., Ohki, K., Ajima, A., Tanaka, S., 1999. Geometrical and topological relationships between multiple functional maps in cat primary visual cortex. Neuroreport 10, 2515–2522.
Li, M., Liu, F., Jiang, H., Lee, T.S., Tang, S., 2017. Long-term two-photon imaging in awake macaque monkey. Neuron 93 (1049-1057), e1043.
Li, M., Song, X.M., Xu, T., Hu, D., Roe, A.W., Li, C.Y., 2019. Subdomains within orientation columns of primary visual cortex. Sci. Adv. 5, eaaw0807.
Livingstone, M.S., Hubel, D.H., 1984. Anatomy and physiology of a color system in the primate visual cortex. J. Neurosci. 4, 309–356.
Maffei, L., Fiorentini, A., 1977. Spatial frequency rows in the straite visual cortex. Vision Res. 17, 257–264.
McLaughlin, D., Shapley, R., Shelley, M., 2003. Large-scale modeling of the primary visual cortex: influence of cortical architecture upon neuronal response. J. Physiol. Paris 97, 237–252.
Molotchnikoff, S., Gillet, P.C., Shumikhina, S., Bouchard, M., 2007. Spatial frequency characteristics of nearby neurons in cats' visual cortex. Neurosci. Lett. 418, 242–247.
Nauhaus, I., Benucci, A., Carandini, M., Ringach, D.L., 2008. Neuronal selectivity and local map structure in visual cortex. Neuron 57, 673–679.
Nauhaus, I., Nielsen, K.J., Disney, A.A., Callaway, E.M., 2012. Orthogonal micro-organization of orientation and spatial frequency in primate primary visual cortex. Nat. Neurosci. 15, 1683–1690.
Ota, K., Oisi, Y., Suzuki, T., Ikeda, M., Ito, Y., Ito, T., Uwamori, H., Kobayashi, K., Kobayashi, M., Odagawa, M., Matsubara, C., Kuroiwa, Y., Horikoshi, M., Matsushita, J., Hioki, H., Ohkura, M., Nakai, J., Oizumi, M., Miyawaki, A., Aonishi, T., Ode, T., Murayama, M., 2021. Fast, cell-resolution, contiguous-wide two-photon imaging to reveal functional network architectures across multi-modal cortical areas. Neuron 109, 1810–1824.
Shoham, D., Hubener, M., Schulze, S., Grinvald, A., Bonhoeffer, T., 1997. Spatio-temporal frequency domains and their relation to cytochrome oxidase staining in cat visual cortex. Nature 385, 529–533.
Silverman, M.S., Grosof, D.H., De Valois, R.L., Elfar, S.D., 1989. Spatial-frequency organization in primate striate cortex. Proc. Natl. Acad. Sci. U. S. A. 86, 711–715.
Sirovich, L., Uglesich, R., 2004. The organization of orientation and spatial frequency in primary visual cortex. Proc. Natl. Acad. Sci. U. S. A. 101, 16941–16946.
Swindale, N.V., 2000. How many maps are there in visual cortex? Cereb. Cortex 10, 633–643.
Tolhurst, D.J., Thompson, I.D., 1982. Organization of neurones preferring similar spatial frequencies in cat striate cortex. Exp. Brain Res. 48, 217–227.
Tootell, R.B., Silverman, M.S., Hamilton, S.L., Switkes, E., De Valois, R.L., 1988. Functional anatomy of macaque striate cortex. V. Spatial frequency. J. Neurosci. 8, 1610–1624.
Wilson, H.R., McFarlane, D.K., Phillips, G.C., 1983. Spatial frequency tuning of orientation selective units estimated by oblique masking. Vision Res. 23, 873–882.
Xu, X., Anderson, T.J., Casagrande, V.A., 2007. How do functional maps in primary visual cortex vary with eccentricity? J. Comp. Neurol. 501, 741–755.